Spatial sequential modeling and predication of global land use and land cover changes by integrating a global change assessment model and cellular automata

Article *in* Earth's Future · April 2019

DOI: 10.1029/2019EF001228

CITATIONS
0

READS
217

7 authors, including:

Min Cao
Nanjing Normal University
16 PUBLICATIONS **74** CITATIONS
SEE PROFILE

Guonian Lü
Key Laboratory of Virtual Geographic Environment, Ministry of Education of PRC, …
153 PUBLICATIONS **1,006** CITATIONS
SEE PROFILE

Min Chen
Key Laboratory of Virtual Geographic Environment, Ministry of Education of PRC
86 PUBLICATIONS **827** CITATIONS
SEE PROFILE

Chen min (Orcid ID: 0000-0001-8922-8789)

Spatial sequential modeling and predication of global land use and land cover changes by integrating a global change assessment model and cellular automata

Min Cao[1,2,3], Yanhui Zhu [1,2,3], Jinling Quan[4], Sheng Zhou[5], Guonian Lü[1,2,3], Min Chen [1,2,3], Mengxue Huang [1,2,3]

1. Key Lab of Virtual Geographic Environment, Ministry of Education of PRC, Nanjing Normal University

2. State Key Laboratory Cultivation Base of Geographical Environment Evolution (Jiangsu Province)

3. Jiangsu Center for Collaborative Innovation in Geographical Information Resource Development and Application

4. State Key Laboratory of Resources and Environmental Information System, Institute of Geographic Sciences and Natural Resources Research, CAS, Beijing 100101, China

5. Institute of Energy Environment and Economy, Tsinghua University, Beijing 100084, China

Corresponding author: Min Chen (chenmin0902@163.com)

Key Points:

1. In this paper, we propose a modeling strategy (hereinafter referred to as GCAM-CA) that combines a global change assessment model (GCAM) with cellular automata (CA);

2. We use this strategy to sequentially spatialize and predict global LUCCs with 1-km spatial resolution and 5-year temporal resolution from 2010 to 2100.

This article has been accepted for publication and undergone full peer review but has not been through the copyediting, typesetting, pagination and proofreading process which may lead to differences between this version and the Version of Record. Please cite this article as doi: 10.1029/2019EF001228

Abstract

Characterizing land use and land cover change (LUCC) is critical for understanding the interaction between human activities and global environmental changes, such as in biological diversity and the carbon cycle. Both natural cycles and human activities can be better examined with more accurate sources of land use data with higher spatial resolution. More importantly, it is crucial to consider spatial heterogeneity to simulate future changes in LUCC. In this paper, a modeling strategy (hereinafter referred to as GCAM-CA) that combines a global change assessment model (GCAM) with cellular automata (CA) is proposed. This modeling strategy is designed to sequentially spatialize global LUCCs with 1-km spatial resolution and 5-year temporal resolution from 2010 to 2100. The GCAM model is employed to predict the land use and land cover area demands for 283 world regions, which are divided by intersecting 32 geopolitical and socioeconomic regions and 18 agro-ecological zones (AEZs). The spatialization rules of CA is trained separately for each world region to distinguish global land use and land cover types. The different spatialization rules and trends in land use and land cover demand for each of the 283 regions reflect the spatial heterogeneity in the GCAM-CA model. We implement and validate the model for the simulation from 2000 to 2010. Next, model is used to simulate three future scenarios, REF, G26 and G45, demonstrating that the GCAM-CA model is effective for future global-scale simulation of LUCCs. GCAM-CA is freely available at the open geographic modeling and simulation platform (OpenGMS, http://geomodeling.njnu.edu.cn/GCAM-CA.jsp).

Keywords: land use and land cover change (LUCC); global change assessment model (GCAM); cellular automata (CA); spatial sequential modeling

1 Introduction

Land use and land cover change (LUCC) is critical for understanding the interaction between human activities and global environmental changes in biological diversity, the carbon cycle, and greenhouse gas emissions (Moss et al., 2010; Hurtt et al., 2011; West et al., 2014). LUCC modeling has proven to be an important tool for analyzing the driving mechanism and spatial distribution of LUCCs in the past and/or possible future (Verburg et al., 2011; Wu et al., 2013; Alexander et al., 2018). LUCC models generally use complex processes to represent land use and land cover on a spatial grid (Verburg et al., 2010; Popp et al., 2017). Global-scale LUCC models are now considered to be crucial inputs for various assessments of anthropogenic environmental change, including climate change, biological diversity and mitigation (Meiyappan et al., 2014; Pelletier et al., 2015; Sleeter et al., 2017; Hirsch et al., 2018; Hanaček et al., 2018; Wolffa et al., 2018).

Despite the fact that global-scale LUCC modeling is required in many situations, few global LUCC models exist due to their complexity (Meiyappan et al., 2014). Originally, most global assessment models involved global-scale land use demand predictions, such as the future agriculture resource model (FARM), Asia-pacific integrated model (AIM), modular applied general equilibrium tool (MAGNET), the parsimonious land use model (PLUM), and the global change assessment model (GCAM). FARM model can allocate land resources by market-clearing prices among competing uses for 13 regions, but not match to specific geographic locations (Darwin et al., 1995; Sands and Leimbach, 2003). AIM/CGE2.0 and MAGNET model are computable general equilibrium models, which can predict land-use

demands for 17 and 26 regions, respectively (Fujimori et al., 2012; Woltjer et al., 2014). PLUM is a simple conceptual model of the socio-economic processes that determine global agricultural land-use change for 157 countries (Engström et al., 2016). GCAM is an integrated, multi-sector model that explores both human and Earth system dynamics for 283 regions (Edmonds et al., 1994).

Representation of land use and land cover at a more detailed spatial resolution is always identified as a critical improvement in global-scale LUCC modeling (Letourneau et al., 2012; Li et al., 2017). For decades, efforts have been made to develop global-scale LUCC models with more detailed spatial resolution. Some models can simulate global-scale land use change with a spatial resolution of 0.5 degree (approximately 55km at the equator), such as the integrated model to assess the greenhouse effect (IMAGE) (Kyle et al., 2011; Doelmana et al., 2018), model of agricultural production and its impacts on the environmen (MAgPIE) (Popp et al., 2014) and cropland and pastureland model (CAPS) (Meiyappan et al., 2014). In addition, there are some models can simulate global-scale land use change with a fine resolution of 5 arc-minutes (approximately 10 km at the equator), including LUSs model (Letourneau et al., 2012), GLOBIOM model (Havlík et al., 2014), CLUMondo model (Van & Verburg, 2014), and LandSHIFT model (Schaldach et al., 2011). This 10-km resolution, however, still produces major distortions in land use patterns because many small urban areas are merged into other land use classes (Li et al., 2017).

Recently, studies have demonstrated that cellular automata (CA) are suitable for the spatial allocation of land use and land cover at a high spatial resolution (Almeida et al., 2008;

Cao et al., 2015). The distinguishing characteristic of CA is that large-scale, complex spatial patterns emerge from its simple small-scale transition rules, which is consistent with complex theories (Clarke et al., 1998; Batty & Torrens, 2005). For decades, CA models have been used to simulate LUCCs at various local or regional scales (Li and Yeh, 2002; Dietzel and Clarke, 2007; Liu et al., 2008; Torrens et al., 2013; Lin et al., 2014), such as in the regional-scale GEOMOD model (Estoque and Murayama, 2012), the continental-scale DynaCLUE model (Verburg and Overmars, 2009), and the continental- to global-scale LandSHIFT model (Schaldach et al., 2011). CA models can also be used to simulate global-scale LUCCs based on land area demand constraints predicted by global assessment models. For example, the FLUS model can simulate global-scale LUCCs by integrating CA and the IMAGE model (Li et al., 2017; Liu et al., 2017; Dong et al., 2018), predicting land use demands for seventeen world regions. The FLUS model can cope with large-scale global LUCC simulations at 1-km spatial resolution. This increase in spatial resolution greatly improves the spatial representation of land use and land cover in global-scale LUCC modeling (Li et al., 2017).

However, refinements are required to properly represent the spatial heterogeneity of land use and land cover in global-scale LUCC models. The spatial heterogeneity of land use and land cover plays an important role in global impact assessments (Meiyappan et al., 2014; Li et al., 2017). For example, regions may have the same climate zone, moisture conditions, soil type and landforms, but have different spatial characteristics of land use and land cover in different countries. Similarly, an entire country may share the same geopolitical and socioeconomic conditions, but still has significant spatial heterogeneity in land use and land

cover due to variations in climate, moisture, soil, or landforms.

Among the global assessment models, the spatial heterogeneity of land use and land cover can be reflected in the GCAM model, which predicts land use and land cover demands for 283 world regions by intersecting 18 agro-ecological zones (AEZs) with temperature bands, humidity, and 32 geopolitical and socioeconomic regions (Page et al., 2016; Calvin et al., 2017). The aim of this study is to present a global-scale LUCC model (hereinafter referred to as GCAM-CA) by integrating GCAM and CA, which allows us to sequentially spatialize global land use and land cover changes with a 1-km spatial resolution and a 5-year temporal resolution from 2010 to 2100. Both natural cycles and human activities are expected to result in spatially heterogeneous land use and land cover within the 283 world regions in the global-scale LUCC model. The GCAM-CA model attempts to use publicly available land use and land cover products to feed most of the global environmental change assessments.

The remainder of this paper is organized into following sections. Section 2 describes the basic structure of the GCAM-CA model, then details the specific methods used to predict land use demand and spatialize land use using CA. Section 3 presents the model application, validation, and scenario simulation. Section 4 conducts model comparison and discussion. Finally, section 5 draws conclusions and considers future areas of research.

2 Methods

2.1 The basic idea of GCAM-CA

As a global integrated assessment model, GCAM expresses the behavior and interactions among five systems: energy, economy, agriculture and land use, water, and climate

(downloaded from: http://www.globalchange.umd.edu/models/gcam/) (Shi et al., 2017). Studies have shown that the GCAM model is useful for exploring the interactions between land use and land cover, social economy, and climate change, and these factors are considered to be suitable for predicting the land use and land cover demands of each AEZ (Wu et al., 2013; Sands and Leimbach, 2003).

In this paper, we constructed the GCAM-CA model by integrating the GCAM model and CA for the spatialization of global land use and land cover changes. The structure of the GCAM-CA model is shown in Figure 1. The GCAM-CA model can be divided into two main parts: (1) prediction of land use demand by the GCAM model for all world regions; and (2) the spatialization of land use and land cover by the CA model. The transition rules of CA are determined using artificial neural network (ANN) methods. Different ANNs are created from training data, after which the well-trained networks are used to estimate the initial probabilities of land conversion on a specific grid cell. The final land use type is confirmed by comparison to the neighborhood influence, conversion weight matrix and other expert experiences.

2.2 Land use demand prediction using GCAM

The agriculture and land use components of the GCAM model consider 283 world regions, which are based on the intersection of two region types: the 18 AEZs and 32 geopolitical and socioeconomic regions (Page et al., 2016; Calvin et al., 2017). The 18 AEZs reflect the natural ecosystems and agricultural activities across the global land area, , accounting for the influence of climate on vegetation and crop productivity (Kyle et al., 2011; Lee, 2005; Chen

et al., 2017). Lands located in a specific AEZ have similar or homogenous soil, landforms and climatic characteristics. The 32 geopolitical and socioeconomic regions represent economic conditions such as industrial production, energy use, trade, and natural resources. In the GCAM model, the 18 AEZs are intersected with the 32 geopolitical regions to generate 283 unique spatial regions, as shown in Figure 2.

In the AgLU component of GCAM, changes in the 283 world regions are modeled based on a range of drivers, including population growth, income, technology improvements, crop productivity, labor costs, energy demand and environmental policies(Vittorio et al., 2016; Snyder et al., 2018). As an integrated assessment model, the land use modeling in GCAM considers comprehensive land use types. Each of the 283 world regions is divided into one of several land categories based on land use and land cover (Kyle et al., 2011). These land use and land cover categories include commercial use types (e.g., bioenergy crops, commercial pasture, cropland, and forest products), as well as non-commercial types (e.g., grassland, shrubland, and non-commercial forestland). Tundra, desert, and built-up land are considered as unavailable for any other uses.

The land allocation methodology used in AgLU includes a market price mechanism, which is defined for crops, animal products and agricultural products (Wise et al., 2014). The land is allocated across agricultural activities to maximize economic returns to the land owners in a region, which is calculated as the revenue minus the production cost, as follows:

$$\pi r_{i,l,p} = y_{i,l,p} \times (P_{i,l} - G_{i,l}) \quad , \quad i\text{= crops, biomass, pasture} \tag{1}$$

where *i, l* and *p* indicate the land use type index, region index and AEZ index,

respectively; $\pi r_{i,l,p}$ and $y_{i,l,p}$ represent the economic return and the yield corresponding to the land use type index *i*, the region index *l* and the AEZ index *p*, respectively; and $P_{i,l}$ and $G_{i,l}$ denote the market price of a product and the non-land cost corresponding to the land use type index *i* and region index *l*, respectively.

For the economic return of forest products, an extra process of earnings conversion from the future to the present is required due to the time delay between planting and harvest. The process is as follows:

$$\pi r_{i,l,p} = \frac{r}{(1+r)^{45}-1} y_{i,l,p} \times (\bar{P}_{i,l} - G_{i,l}), \ i = \text{forest} \quad (2)$$

where *r* represents the interest rate and $\bar{P}_{i,l,m}$ is the price per cubic meter of forest products over three model time periods (45 years) into the future.

A simplified approach is used to allocate the land area in each AEZ with the aim of maximizing profits. Based on the assumptions of the yield distribution function, the share of land use allocated to a given land use type *i* is as follows:

$$S_{i,l} = \frac{\bar{\pi} r_{i,l}^{\ 1/\lambda}}{\sum_p \bar{\pi} r_{i,l,p}^{\ 1/\lambda}}, \quad \lambda > 0 \quad (3)$$

where $S_{i,l}$ and $\bar{\pi} r_{i,l}$ denote the share of land use and the average economic return corresponding to the land use type index *i* and the region index *l*, respectively; λ is a distribution parameter of economic return; and the denominator is the sum of all possible uses for the land.

The land area of a specific type is calculated based on the total land area and the share

of land use, as follows:

$$Landuse_{i,l} = S_{i,l} \times Totalland_l \quad (4)$$

where $Landuse_{i,l}$ represents the land area allocated to land use type i; $S_{i,l}$ denotes the share of allocated land use type i; and $Totalland_l$ is the total land area of region l.

2.3 Spatialization of land use and land cover types using CA

2.3.1 Artificial neural networks (ANNs)

ANNs are nonlinear statistical modeling tools based on biological neural networks. In the ANN approach, the complex relationships or patterns between inputs and outputs are identified through a number of learning-recall iterations (Li and Yeh, 2002; Huang et al., 2018). ANNs have several advantages; most importantly, they can learn from a large number of observational datasets and deliver good performance (Almeida et al., 2008; Omrani et al., 2017).

An ANN with multiple neurons consists of an input layer, none, one or more hidden layers, and an output layer. The input layer contains a group of neurons that are responsible for accepting data imported to the network, such as gross domestic product (GDP), population, temperature, precipitation, and digital elevation model (DEM) data. This concept can be mathematically expressed as follows:

$$X = [x_1, x_2, ..., x_n]^T \quad (5)$$

where x_i denotes the *i*-th neuron of the input layer. In the hidden layer, the signal received by the *j*-th neuron is calculated as follows:

$$net_j(p,t) = \sum_i w_{i,j} \times x_i(p,t) \quad (6)$$

where p and t are the grid cell and training time, respectively; $net_j(p, t)$ is a propagation function that computes the signal of the j-th neuron in the hidden layer; x_i (p, t) is the variable i corresponding to input neuron i; and $w_{i,j}$ represents the adaptive weight between the i-th neuron of the input layer and the j-th neuron in the hidden layer. The number of neurons in the hidden layer is determined according to Kolmogorov´s theorem (Ismailov, 2014). The sigmoid function, viewed as an effective activation function, is selected to determine the connection between hidden and output layers. The formula is as follows:

$$sigmoid(net_j(p,t)) = \frac{1}{1+e^{-net_j(p,t)}} \quad (7)$$

The output layer represents the probability that a current cell would be allocated to any given land use and land cover type. The probability is calculated as follows:

$$P(p,k,t) = \sum_j w_{j,k} \times sigmoid(net_j(p,t)) = \sum_j w_{j,k} \times \frac{1}{1+e^{-net_j(p,t)}} \quad (8)$$

where $P(p, k, t)$ denotes the initial probability that the grid cell p would be identified as the k-th land use and land cover type at training time t; and $w_{j,k}$ represents the adaptive weight between the j-th neuron of the hidden layer and the k-th neuron of the output layer. The training datasets are extracted to train and construct the ANN model, and two adaptive weights $w_{i,j}$ and $w_{j,k}$ are calibrated during the process of training the ANN model.

2.3.2 Conversion weight matrix

The conversion weight matrix of different land types, which indicates the possibility of

conversion between two land use types, is also another important factor that affects land use spatialization. In this study, the conversion weight matrix reflects the probability that the current land use type would be converted to the target land use type in a specific world region, it is calculated from land use data in 2000 and 2010.. Thus, the conversion weight matrices for the 283 world spatial regions differ during the process of land use spatialization.

At each 5-year interval, calculations are performed to allocate different land use and land cover types within a specific world region. The conversion weight matrix for all types of land use varies over time (in Table 1). Thus, the conversion weight matrix can be conceptualized as reflecting the conversion costs of the individual use types.

Table 1. Conversion weight matrix between 10 types of land from 2000 to 2010 (world region 223)

2000 \ 2010	10	20	30	40	50	60	70	80	90	100
10	1.00	0.08	0.65	0.20	0.03	0.01	0.00	0.01	0.01	0.00
20	0.01	1.00	0.27	0.42	0.02	0.02	0.24	0.00	0.02	0.00
30	0.15	0.30	1.00	0.47	0.02	0.01	0.00	0.01	0.05	0.00
40	0.04	0.42	0.44	1.00	0.01	0.01	0.00	0.01	0.07	0.00
50	0.08	0.28	0.19	0.20	1.00	0.12	0.13	0.01	0.01	0.00
60	0.01	0.11	0.06	0.06	0.05	1.00	0.70	0.00	0.01	0.00
70	0.00	0.41	0.00	0.00	0.02	0.25	1.00	0.00	0.00	0.32
80	0.14	0.17	0.25	0.31	0.02	0.02	0.06	1.00	0.03	0.00
90	0.02	0.13	0.38	0.45	0.01	0.01	0.00	0.00	1.00	0.01
100	0.00	0.00	0.01	0.01	0.00	0.00	0.97	0.00	0.01	1.00

*The land use codes 10, 20, …, 100 are defined in Table 2.

2.3.3 Combined probability

The combined probability that a specific cell will be covered by a specific land use type is calculated by integrating the initial probability estimated by ANN, the neighborhood effect, the conversion weight matrix, and the conditional constraints. The equation is as follows:

$$CP_{i,k}^{t} = P_{i,k}^{t} \times \Omega_{i,k}^{t} \times con_{c \to k} \times P_{cons} \times r \quad (9)$$

where $CP_{i,k}^{t}$ denotes the combined probability that a grid cell *i* would be allocated to land use type *k* at iteration time *t*; $P_{i,k}^{t}$ is the initial conversion probability estimated by the ANN model; $\Omega_{i,k}^{t}$ represents the influence of the neighborhood condition, which is calculated dynamically during the iterations; and $con_{c \to k}$ is the conversion weight matrix from land use type *c* to land use type *k*. P_{cons} is the conditional constraints of the transition rules in the GCAM-CA model and *r* is a random variable ranging from 0 to 1. After the model begins running, a grid cell is allocated to the land use type with the highest combined probability.

The workflow for the spatialization of global land use and land cover from 2010 to 2100 for the 283 world regions under different scenarios is shown in Figure 3. The land use demand calculated by GCAM is used to determine whether the next iteration of land use spatialization needs to be performed. When the total area does not meet the requirements of the GCAM model, the process of land use spatialization is continued. The land use type is determined by the combined probability during the process of land use spatialization. The execution of land use spatialization is repeated until the total areas of all land use types reach the land use demands predicted by the GCAM model.

2.4 Coupling between GCAM and CA

In the GCAM-CA model, the GCAM model predicts the land use demands in the 283 world regions at 5-year intervals according to changes in climate, socioeconomic conditions, historical land use and technological progress. The land use demand predictions of the 283 world regions over time are used as the constraint conditions of land use for spatializing the land use and land cover types in the CA model. Additionally, the GCAM model also outputs

GDP and population data, which are used to calibrate the predicted demand of the frozen (unchanged) urban land area in the GCAM model output. Multiple regression methods have proven effective for calibrating the urban demand for GCAM (Dong et al., 2018). The GDP and population data series from 2010 to 2100 are also used as input spatial variables for the CA model. In addition, the global land use and land cover data in the CA model is coupled to the GCAM model and used to calibrate the parameter settings, ensuring consistency between the land use area demand predicted by the GCAM model and the observed land use area in the CA model.

GlobaLand30 (GLC30) is used as the initial land use data in the CA model. This dataset is described in section 3.1. Because of the inconsistency in land use classes between GCAM and GLC30, a classification scheme is required to make the land use classes compatible for simulating and validating the GCAM-CA model. Table 2 lists different classification schemes, including GLC30, GCAM, IMAGE and FLUS.

Table 2. Classification schemes for GLC30, GCAM, IMAGE and FLUS

This study/GLC30	GCAM	IMAGE	FLUS
Cultivated land (10)	Crop Biomass Other arable land	Agricultural land	Farmland
Forest (20)	Managed forest Unmanaged forest	Biofuels Boreal forest Carbon plantations Cool conifer forest Regrowth forest abandonment Regrowth forest timber Temperate deciduous forest Temperate mixed forest Tropical forest Tropical woodland Warm mixed forest	Forest
Shrubland (40)	Shrubland	Scrubland	
Grassland (30)	Grassland Pasture Unmanaged pasture	Extensive grassland Grassland-steppe Savanna	Grassland
Wetland (50)	None	None	Water
Water bodies (60)	None	None	
Urban land (80)	Urban land	None	Urban
Bare land (90)	Rock	Ice	Barren
Permanent snow and ice (100)	Ice Desert	Tundra Hot desert	
Tundra (70)	Tundra	Wooded tundra	

3 Model application and results

The GCAM-CA model introduced in this study can be implemented using the open geographic modeling and simulation platform (OpenGMS, http://geomodeling.njnu.edu.cn/GCAM-CA.jsp). Thus, the model can be employed by users in multiple disciplines to solve complex geographic problems and conduct integrated simulations. In the following section, we use the GCAM-CA model to spatialize the land use and land cover area demand in the integrated assessment framework of GCAM at a 1-km resolution for the period from 2010 to 2100. The global spatialization product for land use prediction in 2050 under the REF scenario is freely available also at the OpenGMS platform.

3.1 Data and spatial variables

GLC30 (http://www.globeland30.org/GLC30Download/) has 10 classes and a resolution of 30 meters for the years 2000 and 2010. These data are used as the initial two periods of LUCC maps for calibration of the GCAM-CA model. GLC30 products include land use and land cover between 80° N and 80° S. The images utilized for classification by GLC30 include TM5 and ETM+ data from the Landsat satellite and multispectral images from the Chinese HJ-1 environmental satellite. The original resolution of 30 meters was first downgraded to 1 km to create the initial land use data for the CA model. The results from GCAM modeling have been verified by previous studies (Zhou et al., 2013, 2018a, 2018b). In 2010, the global land use demand of 126,990 thousand km^2 predicted by GCAM is consistent with the total global land use area of 128,185 thousand km^2 reflected in the GLC30 product (excluding wetlands and water bodies).

Global LUCCs are affected by both anthropogenic and natural drivers (Alexander et al., 2015). In this study, twelve spatial variables (listed in Table 3) are assumed to represent the driving forces of land use change, as commonly used in the global LUCC simulation models (Letourneau et al., 2012; van Asselen and Verburg, 2013; Li et al., 2017). During the experiment, all spatial variables were resampled to the same resolution 1-km in the same projection (World_Goode_Homolosine_Land). The training samples were extracted using a stratified random sampling method to distribute the ten land use classes in the 283 world regions. The training samples account for five percent of the entire global dataset. In total, 6,792,283 samples were collected to train and validate the neural network used to identify the land use and land cover types during the process of spatialization in the GCAM-CA model. Table 3. Spatial variables for training transition rules in GCAM-CA model

Data	Year	Resolution	Source
Population	2010	0.5′	Gridded Population of the World (GPW)
GDP	2010	1°	Global Gridded Geographically Based Economic Data (G-Econ)
distance to road	2010	1km	Global Roads Open Access Data Set
distance to city	2014	1km	10m-cultural-vectors
DEM	2000	0.5′	Global 30 Arc-Second Elevation (GTOPO30)
Slope			Retrieved from DEM
Silt content Clay content pH Sand content	2008	1km	Harmonized World Soil Database
Temperature	1970-2000	0.5′	WorldClim version 1.4(http://worldclim.org)
Precipitation			

A three-layer Multilayer Perceptron (MLP), including an input layer, one hidden layer and an output layer, was utilized to obtain the spatialization rules for identifying the land use and land cover types. The twelve spatial variables and the land use type in 2000 were set as the input layer of MLP for each world region; next, the land use type in 2010 was set as the output layer. To estimate the probability (from 0 to 1), a logistic sigmoid function was utilized in the activation function of the MLP model. Stochastic gradient descent was chosen as the solution for weight optimization. If the loss or score did not improve by at least 0.001, convergence was considered to have been reached and training was halted.

3.2 Model implementation and validation

The GCAM-CA model was implemented in Python and can be run on OpenGMS. The model can compute one of the 283 world regions or the entire global region at a time. To validate the GCAM-CA model, we used the model to simulate changes from 2000 to 2010 and compared the simulated results with the observed GLC30 land use data in 2010. Figure 4 shows the result for 2010 simulated by the GCAM-CA model.

A large number of regions maintained the same land use and land cover type from 2000 to 2010, which leads to high consistency values based on the number of the cells with consistent land use types per grid cell (10×10 km^2). The Figure of Merit index (*FoM*), the ratio of the correct predicted change to the union of the observed and the predicted change, is considered suitable for assessing the accuracy of simulated changes (Pontius, 2008; Li et al., 2017). Therefore, we also used the *FoM* index to validate the global LUCC simulation from 2000 to 2010. The formula is as follows:

$$FoM = \frac{B}{A+B+C+D} \tag{10}$$

where *A* denotes the total number of observed changed cells that are predicted to be unchanged cells; *D* denotes the total number of observed unchanged land use cells simulated as changed cells; and *B* and *C* are the total number of observed changed cells that are predicted to be changed cells with correct and incorrect land use types, respectively.

Figure 5 shows the spatial distribution of *FoM* values in the 283 regions for the 2000 to

2010 global land use simulation made using the GCAM-CA model. The *FoM* values of the 283 regions range from 10 to 46%, which is similar to the results of other simulation models. For instance, the *FoM* values of the FLUS model for global land use simulation range from 10 to 29% (Li et al., 2017). Figure 5 highlights the spatial heterogeneity of *FoM* values in different regions. The areas with greater human activity and complex LUCCs tend to have lower *FoM* values, which are indicated by pink and light purple colors in Figure 5. Conversely, areas with less human activity and LUCCs, such as the Sahara Desert, tend to have higher *FoM* values, which are shown in orange and brown colors in Figure 5.

3.3 Scenario simulation from 2010 to 2100

A scenario-based LUCC simulation can help assess potential land use change in an uncertain future (Sohl et al., 2012; Li et al., 2017). In this study, the GCAM model outputs global land use area for the 283 world regions under three policy scenarios, REF, G26 and G45. REF is the reference scenario, which assumes no changes in climate policy but considers factors such as technological progress. G26 and G45 are selected from the representative concentration pathway (RCP) scenarios from 2005 to 2100 (Kawase et al., 2011; Vuuren et al., 2011). The G26 and G45 scenarios have the same population and income drivers as the GCAM reference scenario, but apply greenhouse gas emission valuation policies. G45 stabilizes atmospheric radiative forcing at 4.5 W m^{-2} in 2100 and temperature changes within 3ºC; this scenario is widely accepted as likely. G26 stabilizes radiative forcing at 2.6 W m^{-2} in the year 2100 and assumes that value is never exceeded; it caps the global average temperature rise at 2ºC. This scenario represents a radical reduction in radiative forcing. At

present, the G26 scenario is considered difficult to achieve.

In the GCAM model, non-arable lands including water bodies and wetlands are not tracked; desert, tundra, and urban areas are tracked but considered to be fixed. The series of urban area predictions from 2015 to 2100 are revised according to the population and GDP data obtained from the GCAM model output, although the proportion of urban land area remains at approximately 1%. The areas of the four major LUCC classes, including cultivated land, forest, grassland and shrubland, are predicted for the period from 2010 to 2100 under the three policy scenarios in the GCAM model (Figure 6). Cultivated land is a major land use that affects food production and ecological systems. The area of cultivated land increases from 2010 to 2100 in all three scenarios, as shown in Figure 6(a). In contrast, the areas of forest, grassland and shrubland decrease at a global scale, as shown in Figures 6(b)-(d).

As shown in Figure 6, the changes in area of the four major LUCC classes are smallest under the REF scenario, largest for the G26 scenario, and intermediate for the G45 scenario. The area predictions for the different scenarios verify the assumptions of each scenario: in the G26 scenario, the amount of human-used land (e.g., cultivated land) should be maximized, which is generally true; in the REF scenario, where no climate policy interventions take place, the amount of human-used land should be minimized and natural areas (e.g., forest, grassland and shrubland) protected, which generally occurs. The scenario simulations can help estimate future global LUCC, especially in the face of uncertainty (Hurtt et al., 2011).

Land use dynamics are represented by the percentages of land use and land cover

changes, which are calculated by counting up the total number of changes between different land use types per grid cell (10×10 km^2). Four typical regions are selected to illustrate land use patterns at a finer resolution, because patterns at a global scale are difficult to show explicitly. The change in the percentages of four major land use types in four typical regions are shown in Figure 7.

Figure 7(a) shows the percentage change in cultivated land of a typical region in eastern Asia, where there are large tracts of cultivated land. Among the three scenarios, there are greater increases in agricultural land from 2010 to 2050 under the G26 and G45 scenarios than for the REF scenario. Figure 7(b) depicts a typical region with dense forest in India. Greater decreases in forest occur under the G26 and REF than for the G45 scenario from 2010 to 2050. Figure 7(c) depicts a region in southern Africa with a large amount of grassland. There are slight reductions in grassland area under all three scenarios, though the reductions under the G26 and G45 scenarios are larger than for the REF scenario. Figure 7(d) shows reductions in shrubland in South America under all three scenarios, with the greatest changes occurring in the G26 scenario. Overall, changes in the four major land use types are greatest under the G26 scenario, least for the REF scenario, and intermediate for the G45 scenario.

4 Comparison and discussion

The IMAGE and FLUS models can provide global land use simulations at a fine resolution, and both models are available for public use. In this study, we focus on verifying whether the GCAM-CA simulations are consistent with those generated by the FLUS model at a 1-km spatial resolution. The GCAM-CA products under the REF scenario are compared with the

FLUS products under scenario A1B, both in 2050 (in Table 5). The GCAM-CA model contains six of the same land use types as the FLUS model (water, forest, grassland, farmland, urban areas, and barren areas) and four land use types that are not included in the FLUS model (shrubland, wetland, tundra and areas with permanent snow and ice). The areas with the six land use types that are consistent between models are examined for inter-model consistency.

Table 4. Consistency between the products generated by GCAM-CA and FLUS in 2050

GCAM-CA / Flus	Water	Forest	Grassland	Farmland	Urban	Barren
Water	**0.639**	0.127	0.135	0.093	0.436	0.008
Forest	0.075	**0.563**	0.062	0.139	0.064	0.004
Grassland	0.202	0.221	**0.487**	0.231	0.096	0.085
Farmland	0.001	0.007	0.001	**0.363**	0.004	0.001
Urban	0.030	0.004	0.004	0.009	**0.362**	0.002
Barren	0.053	0.078	0.311	0.165	0.038	**0.900**
Total accuracy	0.61					
Kappa	0.49					

Table 4 shows the percent consistency in 2050 for each of the six comparable land use types between the products generated by GCAM-CA and FLUS. In total, 63.9% of the water area in GCAM-CA is also classified as water in FLUS. The percent consistency of forest, grassland, farmland, urban and barren areas is 56.3%, 48.7%, 36.3%, 36.2% and 90.0%, respectively. The total accuracy and kappa values are 0.61 and 0.49, respectively, which indicate that the two results are generally consistent. However, there is a number of major differences between the modeling results. For example, 22.1% of forest areas in GCAM-CA are simulated as grassland in FLUS and 31.1% of grassland areas are simulated as barren. There are similar inconsistencies between farmland and grassland in the GCAM-CA and FLUS

simulations.

In the GCAM-CA model, the different spatialization rules and different land use and land cover demand predictions for the 283 world regions reflect the spatial heterogeneity accounted for by the model. To properly represent the spatial heterogeneity of the land use and land cover changes, a more detailed classification scheme of land use and land cover is required. Data sources with a higher spatial resolution can greatly reduce confusion between land use and land cover classes and can help better express land use information.

5 Conclusion

In this study, we developed GCAM-CA, is available for public use. This model is a global-scale LUCC model that sequentially spatializes land use and land cover with a 1-km spatial resolution and a 5-year temporal resolution from 2010 to 2100 under three policy scenarios of REF, G45 and G26. The CA methodology was applied to spatialize global land use and land cover types based on the constraints of land use area demand predicted by the GCAM model for the 283 spatial regions over the global. The spatialization rules in the CA process and the LUCC trends in the GCAM model account for the spatial heterogeneity in land use and land cover. The results of *FoM* show that calculating the spatialization in this partitioned manner can improve the accuracy of the simulation results. Three policy scenarios of REF, G45 and G26, were used in the GCAM framework to assess global LUCC changes under various possible futures. The GCAM model simulates GDP and population for every 5-year interval from 2010 to 2100. These outputs are used to revise the demand predictions for urban lands in the GCAM model. Additionally, these outputs are used as spatial variables, so that GDP and population change dynamically during the GCAM-CA model simulations over

time.

In future research, global LUCC products with higher spatial resolution and accuracy may be possible. Although the GLC30 products used in this study have up to 30-m resolution, most of the spatial variable datasets that are available for public download have a maximum resolution of only 1 km, so spatialization can only be executed at a 1-km resolution. And all datasets used in the GCAM-CA model are converted to the Goode Homolosine projection(land), which is a pseudo-cylindrical, equal-area, composite projection often used for world maps. While this projection can minimize area errors at high latitudes, errors will still be present. The GCAM-CA model may be further improved by executing it on a sphere, which can help reduce area errors at high latitudes.

Acknowledgements

We would like to thank the editor and anonymous reviewers for giving helpful comments, corrections, and suggestions on how to improve the paper. GCAM-CA is freely available at the open geographic modeling and simulation platform (OpenGMS, http://geomodeling.njnu.edu.cn/GCAM-CA.jsp).

Funding

This study was supported by the National Basic Research Program of China (973 Program) (No. 2015CB954101, No.2015CB954103), the National Science Foundation of China (Grant No. 41671385, Grant No. 41622108, Grant No. 41871178), Surveying mapping and geoinformation research project of Jiangsu Province (No.JSCHKY201814), and the Priority Academic Program Development of Jiangsu Higher Education Institutions (No. 164320H116).

References

(1) Alexander, P., Rounsevella, M. D. , Dislichc, C., Dodsone, J. R., Engströmf, K., Moran, M. (2015). Drivers for global agricultural land use change: The nexus of diet, population, yield and bioenergy. *Global Environmental Change*, **35**, 138-147.

(2) Alexander, P., Rabin, S., Anthoni, P., Henry, R., Pugh, T. A. M., Rounsevell, M. D. A., et al. (2018). Adaptation of global land use and management intensity to changes in climate and atmospheric carbon dioxide. *Global Change Biology*, **24**(7), 2791-2809.

(3) Almeida, C. M., Gleriani, J. M., Castejon, E. F., Soares-Filho, B. S. (2008). Using neural networks and cellular automata for modelling intra-urban land-use dynamics. *International Journal of Geographical Information Science*, **22** (9), 943-963.

(4) Batty, M., Torrens, P. M. (2005). Modelling and prediction in a complex world. *Futures*, **37** (7), 745-766.

(5) Calvin, K.,Wise, M., Kyle, P., Clarke, L., Edmonds, J. (2017) A hindcast experiment using the GCAM 3.0 agriculture and land-use module. *Climate Change Economics*, **8** (1), 1962-1970.

(6) Cao, M., Tang, G., Shen, Q., Wang, Y. (2015) A new discovery of transition rules for cellular automata by using cuckoo search algorithm. *International Journal of Geographical Information Science*, **29** (5), 806–824.

(7) Chen, M., Vernon, C. R., Huang, M., Calvin, K. V., Page, Y. L., Kraucunas, I. (2017). Exploring Land Use and Land Cover Change and Feedbacks in the Global Change Assessment Model. *In the AGU Fall Meeting Abstracts*.

(8) Clarke, K. C., Gaydos, L. J. (1998). Loose-coupling a cellular automata model and GIS: long-term urban growth prediction for San Francisco and Washington/Baltimore. *International Journal of Geographical Information Science*, **12** (7), 699-714.

(9) Darwin, R., Tsigas, M. E., Lewandrowski, J., Raneses, A. (1995). *World agriculture and climate change: economic adaptations* (No. 1473-2016-120700).

(10) Dietzel, C., Clarke, K. C. (2007) Toward optimal calibration of the SLEUTH land use change model. *Transactions in GIS*, **11** (1), 29-45.

(11) Doelmana, J. C., Stehfesta, E., Tabeaub, A., Meijl, H. V., Lassalettaa, L., Gemaat, D. E. H. J., et al. (2018). Exploring SSP land-use dynamics using the IMAGE model: Regional and gridded scenarios of land-use change and land-based climate change mitigation. *Global Environmental Change,* **48**, 119-135.

(12) Dong, N., You, L., Cai, W., Li, G., Lin, H. (2018). Land use projections in China under global socioeconomic and emission scenarios: Utilizing a scenario-based land-use change assessment framework. *Global Environmental Change*, **50**, 164-177.

(13) Edmonds,J. A., Wise, M. A., MacCracken, C. N. (1994). Advanced energy technologies and climate change: An analysis using the global change assessment model (GCAM) (No. PNL-9798). Pacific Northwest National Lab.(PNNL), Richland, WA (United States).

(14) Engström K, Rounsevell M D A, Murray-Rust D, et al. (2016). Applying Occam's razor to global agricultural land use change. Environmental modelling & software, 75: 212-229.

(15) Estoque, R. C., Murayama, Y. (2012). Examining the potential impact of land use/cover changes on the ecosystem services of Baguio city, the Philippines: A scenario-based analysis. *Applied Geography*, **35** (1-2), 316-326.

(16) Fujimori, S., Hasegawa, T., Masui, T., Takahashi, K., 2014. Land use representation in a global CGE model for long-term simulation: CET vs. logit functions. Food Secur. 6, 685–699.

doi:http://dx.doi.org/10.1007/s12571-014-0375-z.
(17) Hanaček, K., Rodríguez-Labajos, B. (2018). Impacts of land-use and management changes on cultural agroecosystem services and environmental conflicts—a global review. *Global Environmental Change*, **50**, 41-59.
(18) Havlík, P., Valin, H., Herrero, M., et al. (2014).Climate change mitigation through livestock system transitions. Proceedings of the National Academy of Sciences, 111(10): 3709-3714.
(19) Hirsch, A. L., Guillod, B. P., Seneviratne, S. I., Beyerle, U., Boysen, L. R., Brovkin, V., et al. (2018). Biogeophysical Impacts of Land-Use Change on Climate Extremes in Low-Emission Scenarios: Results From HAPPI-Land. *Earth's Future*, **6**(3), 396-409.
(20) Huang, B., Zhao, B., Song, Y. M. (2018) Urban land-use mapping using a deep convolutional neural network with high spatial resolution multispectral remote sensing imagery. *Remote Sensing of Environment*, **214**, 73-86.
(21) Hurtt, G. C., Chini, L. P., Frolking, S., Betts, R. A., Feddema, J., Fischer, G., et al. (2011). Harmonization of land-use scenarios for the period 1500–2100: 600 years of global gridded annual land-use transitions, wood harvest, and resulting secondary lands. *Climatic change,* **109** (1-2), 117.
(22) Ismailov, V. E. (2014). On the approximation by neural networks with bounded number of neurons in hidden layers. Journal of Mathematical Analysis and Applications, 417(2), 963-969.
(23) Kawase, H., Nagashima, T., Sudo, K., Nozawa, T. (2011). Future changes in tropospheric ozone under representative concentration pathways (rcps). *Geophysical Research Letters*, **38**(38), 359-378.
(24) Kyle, G. P., Luckow, P., Calvin, K. V., Emanuel, W. R., Nathan, M., Zhou, Y. (2011). GCAM 3.0 agriculture and land use: data sources and methods. Pacific Northwest National Lab (PNNL) Richland, WA (United States).
(25) Lee, H. L. (2005). Incorporating agro-ecologically zoned land use data and landbased greenhouse gases emissions into the GTAP framework. *In the 8th Annual Conference on Global Economic Analysis. Lübeck, Germany*. http://nccur.lib.nccu.edu.tw/handle/140.119/74733.
(26) Letourneau, A., Verburg, P. H., Stehfest, E. (2012). A land-use systems approach to represent land-use dynamics at continental and global scales. *Environmental Modelling and Software,* **33** (5), 61-79.
(27) Li, X., Chen, G., Liu, X., Liang, X., Wang, S., Chen, Y., et al. (2017). A New Global Land-Use and Land-Cover Change Product at a 1-km Resolution for 2010 to 2100 Based on Human–Environment Interactions. *Annals of the American Association of Geographers*, 1-20.
(28) Li, X., Yeh, A. G. (2002). Neural-network-based cellular automata for simulating multiple land use changes using GIS. *International Journal of Geographical Information Science,* **16** (4), 323–343.
(29) Lin, J., Huang, B., Chen, M., Huang, Z. (2014). Modeling urban vertical growth using cellular automata—Guangzhou as a case study. *Applied Geography,* **53**, 172-186.
(30) Liu, L., Li, X., Liu, L., He, J., Ai, B. (2008). A bottom-up approach to discover transition rules of cellular automata using ant intelligence. *International Journal of Geographical Information Science,* **22** (11-12), 1247-1269.
(31) Liu, X., Liang, X., Li, X., Xu, X., Ou, J., Chen, Y., et al. (2017). A future land use simulation model (FLUS) for simulating multiple land use scenarios by coupling human and natural effects. *Landscape Urban Plan*, **168**, 94–116.
(32) Meiyappan, P., Dalton, M., O'Neill, B. C., Jain, A. K. (2014). Spatial modeling of agricultural land-use change at global scale. *Ecological Modelling,* **291**, 152–74.
(33) Moss, R. H., Edmonds, J. A., Hibbard, K. A., Manning, M. R., Rose, S. K., van Vuuren, D. P., et al. (2010). The next generation of scenarios for climate change research and assessment. *Nature*, **463** (7282), 747.

(34) Omrani, H., Tayyebi, A., Pijanowski, B. (2017). Integrating the multi-label land-use concept and cellular automata with the artificial neural network-based Land Transformation Model: an integrated ML-CA-LTM modeling framework. *GIScience & Remote Sensing,* **54** (3), 283-304.
(35) Page, Y. L., West, T. O., Link, R., Patel, P. (2016). Downscaling land use and land cover from the Global Change Assessment Model for coupling with Earth system models. *Geoscientific Model Development,* **9** (9), 3055-3069.
(36) Pelletier, J. D., Murray, A.B., Pierce, J.L., Bierman, P.R., Breshears, D. D., Crosby, B. T., et al. (2015). Forecasting the response of Earth's surface to future climatic and land use changes: A review of methods and research needs. *Earth's Future*, **3**(7): 220-251.
(37) Pontius, R. G., Boersma, W., Castella, J. C., Clarke, K., de Nijs, T., Dietzel, C., et al. (2008). Comparing the input, output, and validation maps for several models of land change. *The Annals of Regional Science*, **42**(1), 11-37.
(38) Popp, A., Calvin, K., Fujimori, S., Havlik, P., Humpenöder, F., Stehfest, E., et al. (2017). Land-use futures in the shared socio-economic pathways. *Global Environmental Change*, **42**, 331-345.
(39) Popp, A., Humpenöder, F., Weindl, I., Bodirsky, B. L., Bonsch, M., Lotze-Campen, H., et al. (2014). Land-use protection for climate change mitigation. *Nature Climate Change*, **4**(12), 1095.
(40) Prestele, R., Alexander, P., Rounsevell, M. D., Arneth, A., Calvin, K., Doelman, J., et al. (2016). Hotspots of uncertainty in land-use and land-cover change projections: a global-scale model comparison. *Global change biology*, **22**(12), 3967-3983.
(41) Sands, R. D., Leimbach, M. (2003). Modeling agriculture and land use in an integrated assessment framework. *Climatic Change*, **56** (1-2), 185-210.
(42) Schaldach, R., Alcamo, J., Koch, J., Kölking, C., Lapola, D. M., Schüngel, J., Priess, J. A. (2011). An integrated approach to modelling land-use change on continental and global scales. *Environmental Modelling and Software,* **26** (8), 1041–51.
(43) Shi, W., Ou, Y., Smith, S. J., Ledna, C. M., Nolte, C. G., Loughlin, D. H. (2017). Projecting state-level air pollutant emissions using an integrated assessment model: GCAM-USA. *Applied Energy,* **208**, 511-521.
(44) Snyder, A. C., Link, R. P., Calvin, K. V. (2018). Evaluation of integrated assessment model hindcast experiments: a case study of the GCAM 3.0 land use module. *Geoscientific Model Development Discussions,* **10** (12), 1-19.
(45) Sleeter, B. M., Tamara S. Wilson, Ethan Sharygin, Jason T. Sherba. (2017). Future Scenarios of Land Change Based on Empirical Data and Demographic Trends. *Earth's Future*, **5**(11): 1068-1083. https://doi.org/10.1002/2017EF000560
(46) Sohl, T. L., Sleeter, B. M., Sayler, K. L., Bouchard, M. A., Reker, R. R., Bennett, S. L., et al. (2012). Spatially explicit land-use and landcover scenarios for the Great Plains of the United States. *Agriculture, Ecosystems & Environment*, **153** (6087), 1–15.
(47) Torrens, P. M., Kevrekidis, Y., Ghanem, R., Zou, Y. (2013). Simple urban simulation atop complicated models: multi-scale Equation-Free computing of sprawl using geographic automata. *Entropy*, **15** (7), 2606-2634.
(48) Van Asselen, S., Verburg, P. H. (2014). Land cover change or land-use intensification: simulating land system change with a global-scale land change model. *Global Change Biology*, **19** (12), 3648-3667.
(49) Verburg, P. H., Overmars, K. P. (2009). Combining top-down and bottom-up dynamics in land use modeling: exploring the future of abandoned farmlands in Europe with the Dyna-CLUE model. *Landscape Ecology,* **24** (9), 1167.
(50) Verburg, P. H., van Berkel, D. B., van Doorn, A. M., van Eupen, M., van den Heiligenberg, H. A. (2010).

Trajectories of land use change in Europe: a model-based exploration of rural futures. Landscape ecology, 25(2), 217-232.

(51) Verburg, P. H., Ellis, E. C., Letourneau, A. (2011). A global assessment of market accessibility and market influence for global environmental change studies. Environmental Research Letters, 6(3), 1-12.

(52) Vittorio, A. V. D., Kyle, P., Collins, W. D. (2016). What are the effects of Agro-Ecological Zones and land use region boundaries on land resource projection using the Global Change Assessment Model? *Environmental Modelling & Software,* **85**, 246-265.

(53) Vuuren, D. P. V., Stehfest, E. , Elzen, M. G. J. D., Kram, T., Vliet, J. V., Deetman, S., et al. (2011). Rcp2.6: exploring the possibility to keep global mean temperature increase below 2°c. *Climatic Change*, **109(**1-2), 95-116.

(54) West, T. O., Page, Y. L., Huang, M., Wolf, J., Thomson, A. M. (2014). Downscaling global land cover projections from an integrated assessment model for use in regional analyses: results and evaluation for the US from 2005 to 2095. *Environmental Research Letters,* **9** (6), 1-15.

(55) Wise, M., Dooley, J., Luckow, P., Calvin, K., Kyle, P. (2014). Agriculture, land use, energy and carbon emission impacts of global biofuel mandates to mid-century. *Applied Energy*, **114**, 763-773.

(56) Wolffa, S., Schrammeijera, E. A., Schulpa, C. J. E., Verburg, P. H. (2018). Meeting global land restoration and protection targets: What would the world look like in 2050? *Global Environmental Change,* **52**, 259-272.

(57) Woltjer, G. B., Kuiper, M., Kavallari, A., van Meijl, H., Powell, J. P., Rutten, M. M. et al. (2014). The MAGNET model: module description (No. 14-57). LEI Wageningen UR.

(58) Wu, F., Zhan, J., Xu, Q., Xiong, Y., Sun, Z. (2013). A comparison of two land use simulation models under the RCP4. 5 Scenario in China. *Advances in Meteorology*, 1-7. http://dx.doi.org/10.1155/2013/578350.

(59) Zhou, S., Kyle, G. P., Yu, S., Clarke, L. E., Eom, J., Luckow, P., et al. (2013).Energy use and CO^2 emissions of China's industrial sector from a global perspective. *Energy Policy*, **58**, 284-294.

(60) Zhou, S., Wang, Y., Yuan, Z., Ou, X. (2018a). Peak energy consumption and CO^2 emissions in China's industrial sector. *Energy Strategy Reviews*, **20**, 113-123.

(61) Zhou, S., Wang, Y., Zhou, Y., Clarke, L. E., Edmonds, J. A. (2018b). Roles of wind and solar energy in China's power sector: Implications of intermittency constraints. *Applied Energy,* **213**, 22-30.

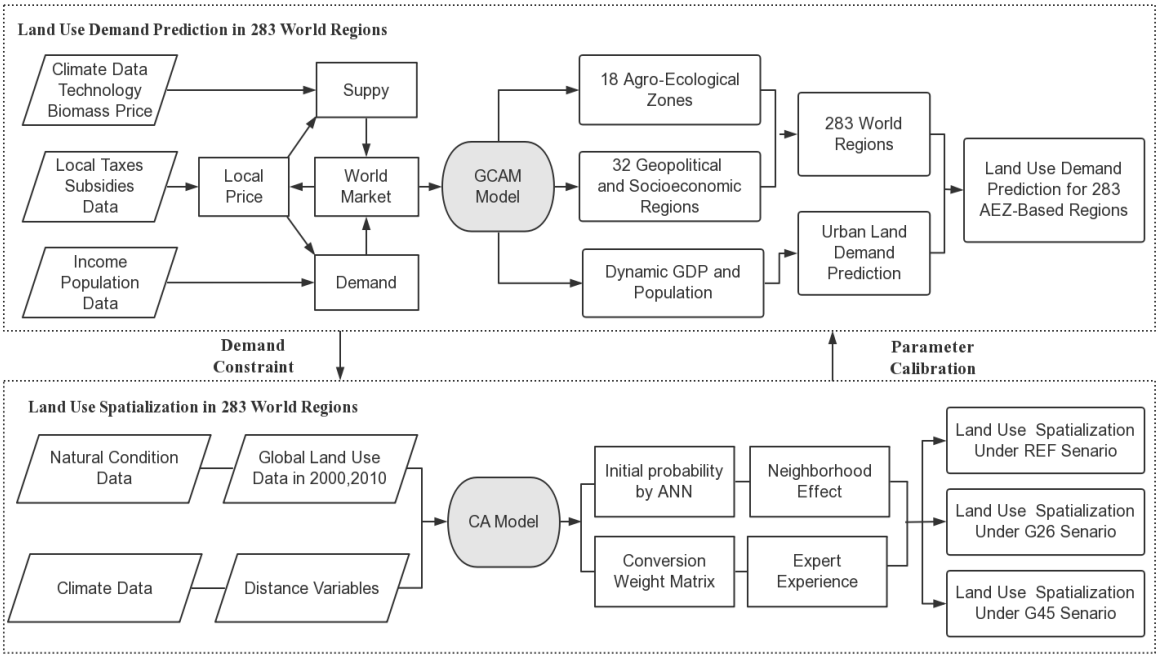

Figure 1. Basic framework of the GCAM-CA model.

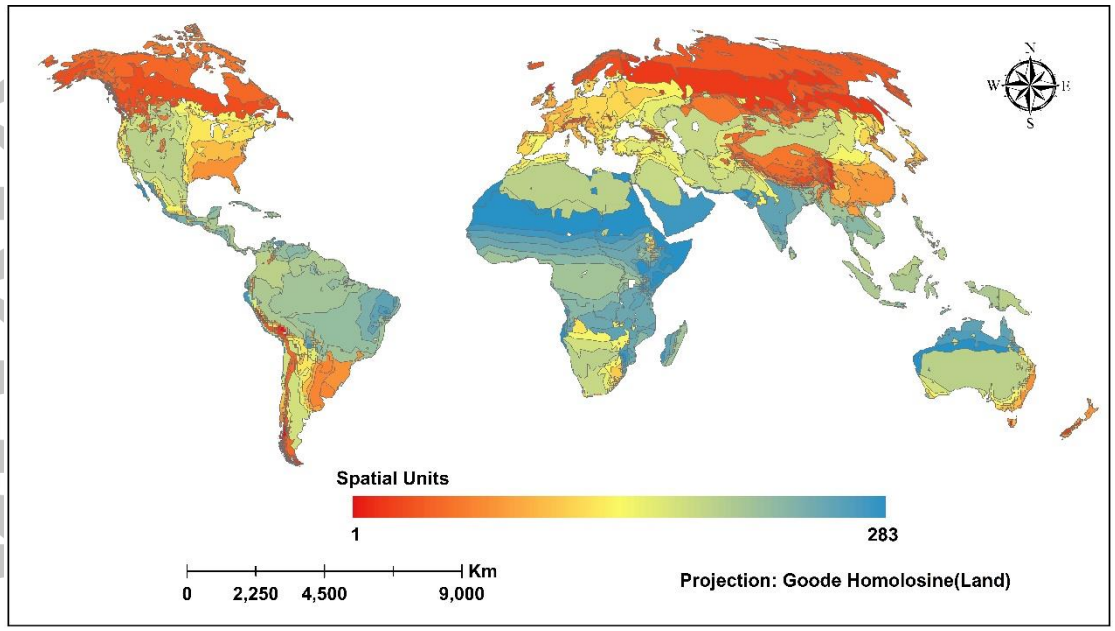

Figure 2. Global spatial distribution of 283 world regions (data source: http://www.globalchange.umd.edu/gcam).

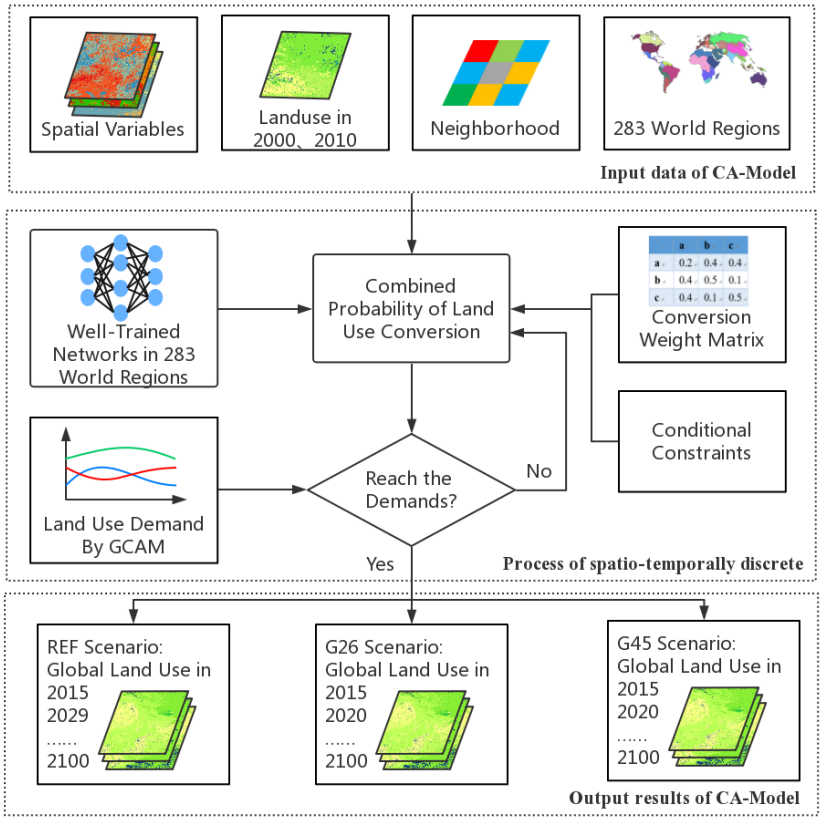

Figure 3. Workflow of the CA spatialization.

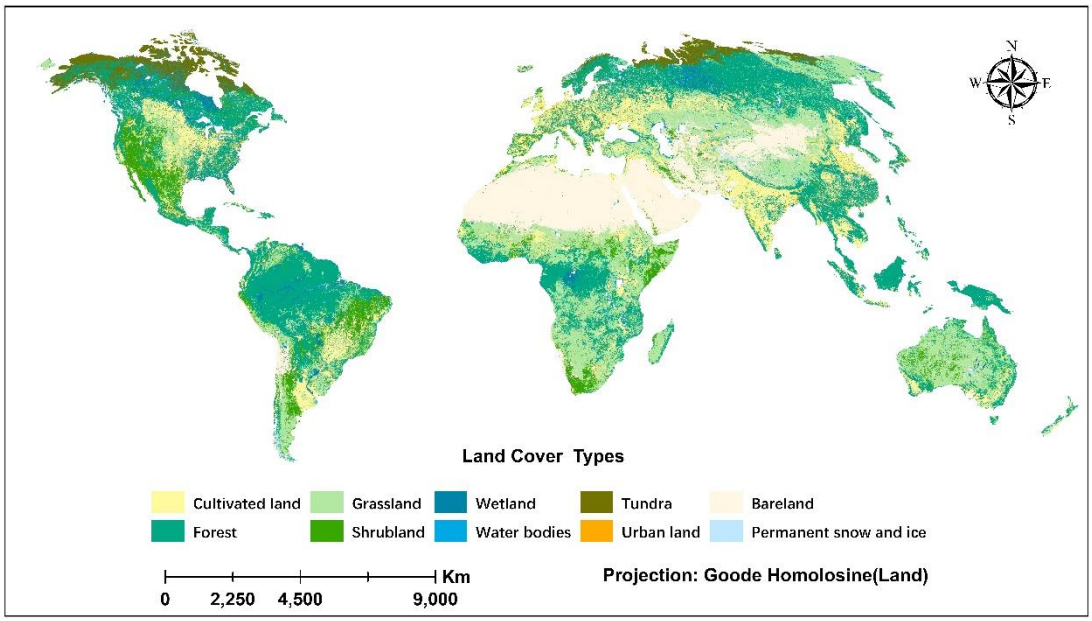

Figure 4. GCAM-CA simulation results for 2010.

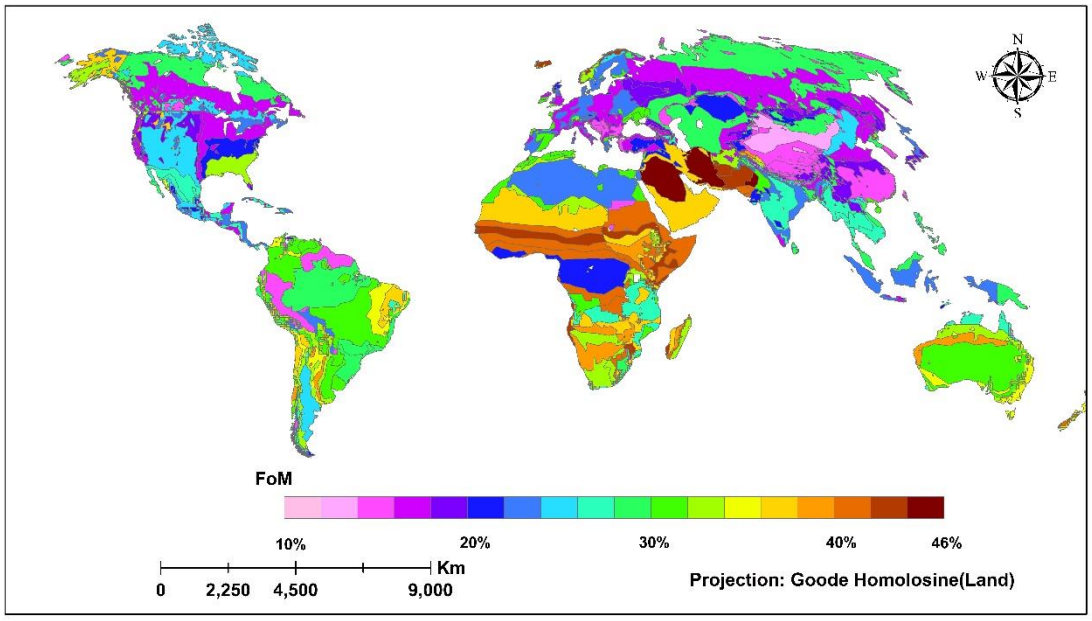

Figure 5. Spatial distribution of *FoM* values for the 283 world regions for the 2010 GCAM-CA simulation results.

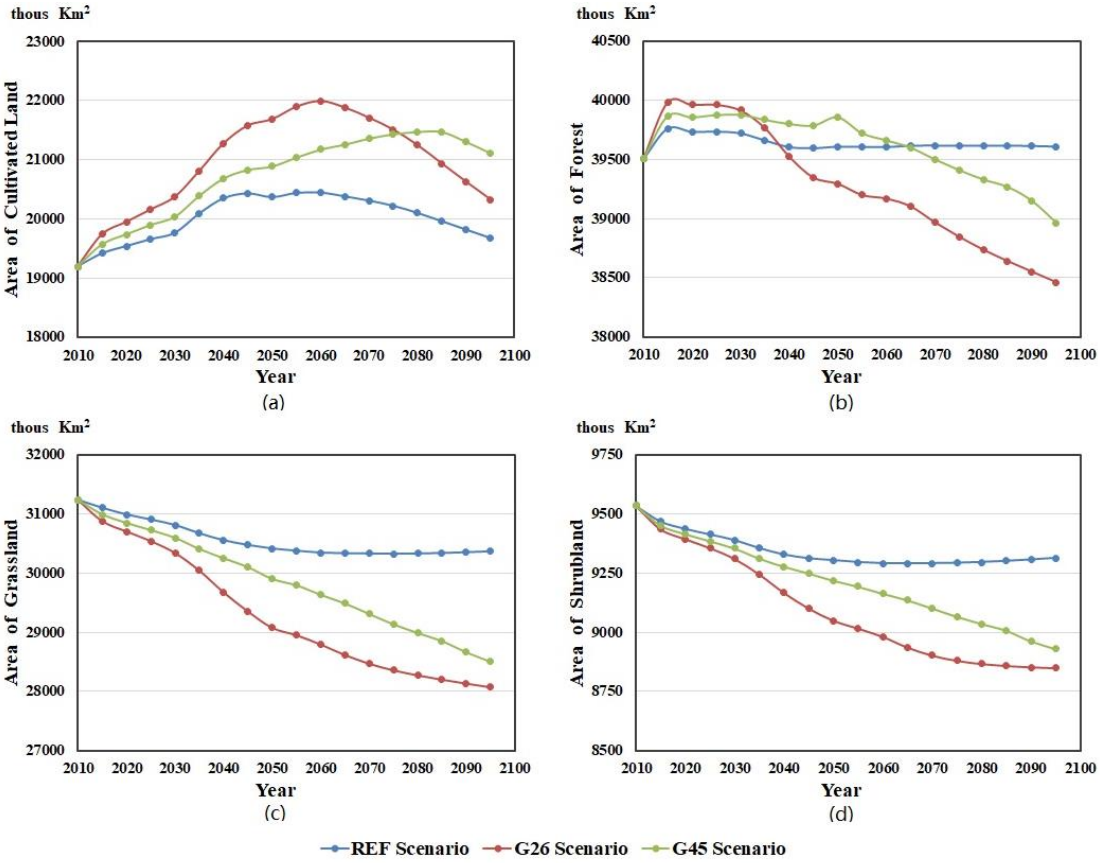

Figure 6. Simulations of the four major LUCC classes under all three scenarios in the GCAM model.

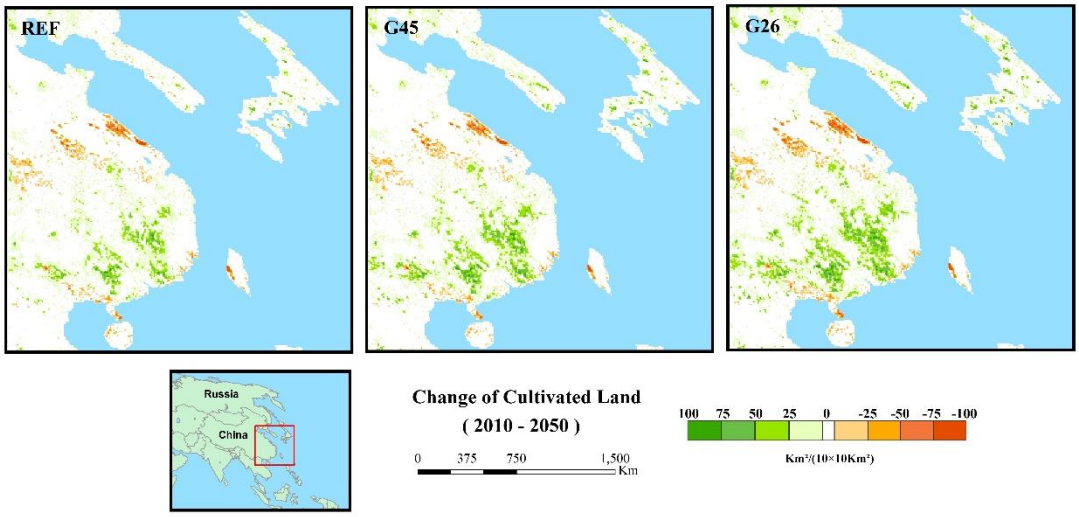

(a) Change percentage of cultivated land in a subregion in eastern of Asia

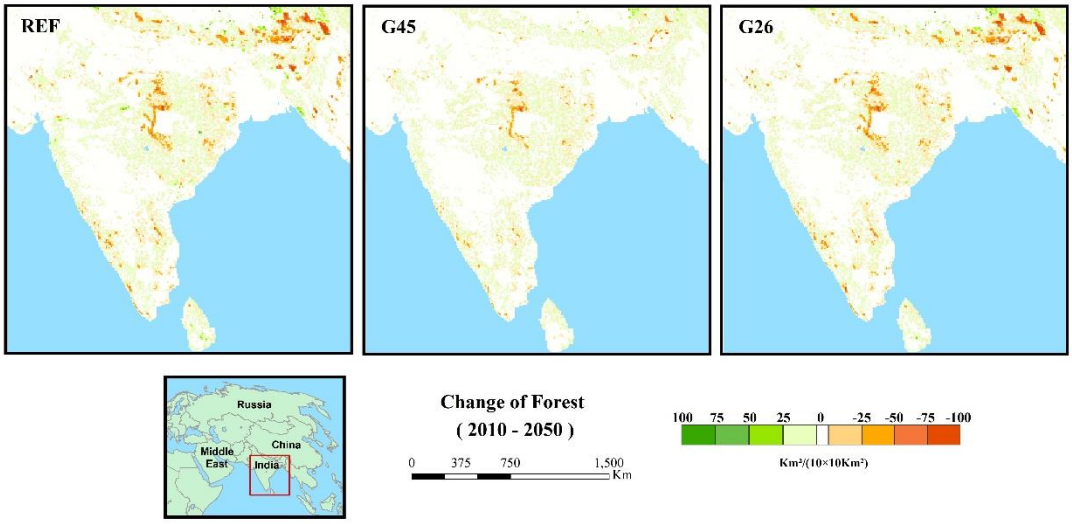

(b) Change percentage of forest in a subregion in western of Asia

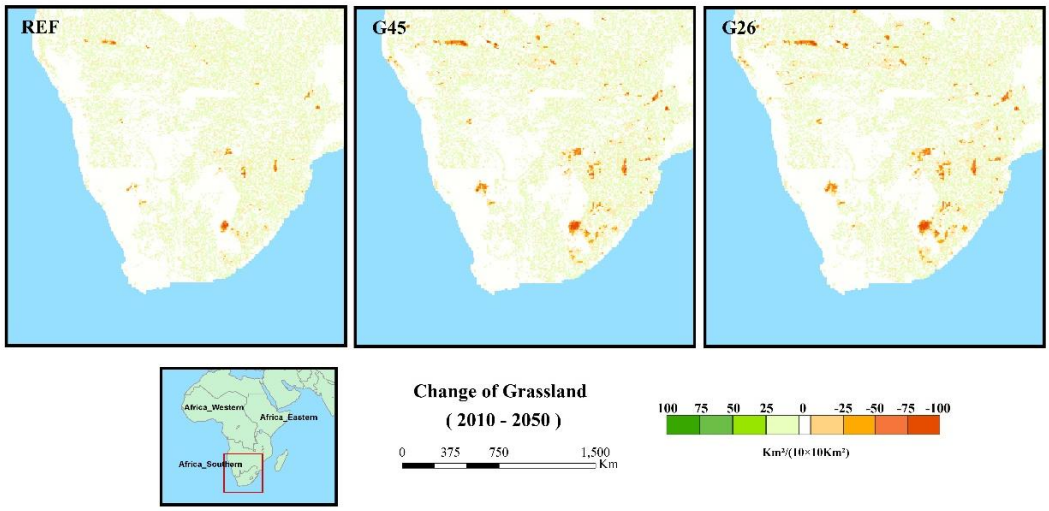

(c) Change percentage of grassland in a subregion in south of Africa

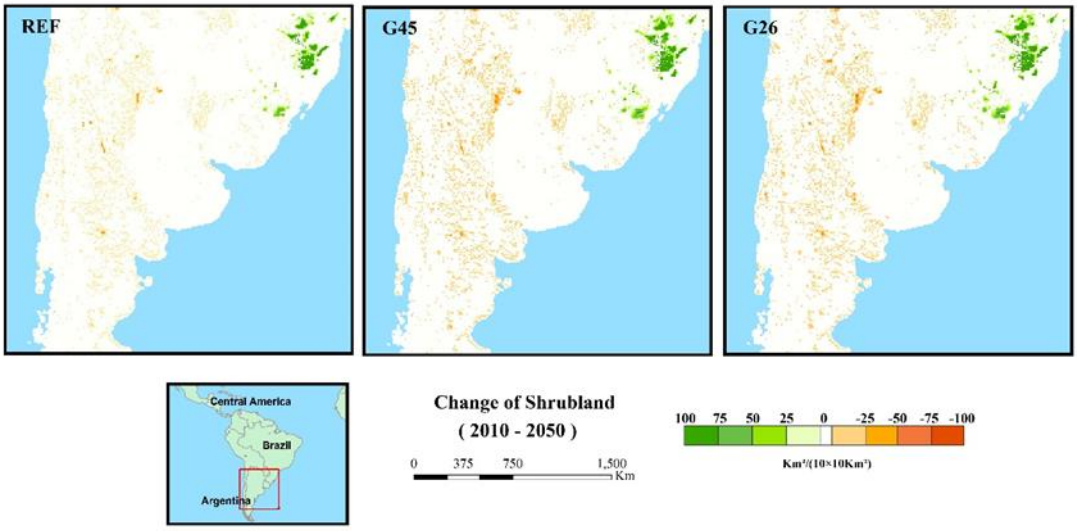

(d) Change percentage of shrubland in a subregion in South America

Figure 7. Percentage change in major land use types in four typical regions for the three scenarios from 2010 to 2050.